

Photometric Observations Using Orthogonal Transfer CCDs

Steve B. Howell

WIYN Observatory and National Optical Astronomy Observatories,
950 N. Cherry Ave, Tucson, AZ 85719

Mark E. Everett

Astrophysics Group, Planetary Science Institute, 620 N. 6th Ave, Tucson, AZ 85705

John L. Tonry & Andrew Pickles

Institute for Astronomy, University of Hawaii, Honolulu, HI 96822

and

Courtney Dain

IGPP, University of California, Riverside, CA 92521

Received _____; accepted _____

Submitted to the P.A.S.P.

ABSTRACT

Orthogonal Transfer CCDs were developed to compensate for real-time image motion, essentially providing tip/tilt corrections without additional optics or moving parts. Due to the complex gate structures of OTCCDs, it was unclear as to their ability to provide high precision photometric observations and their use as high speed photometers. We detail new observations obtained with the OPTIC camera at the UH 2.2-m telescope on Mauna Kea which explore both of these areas. We find that OTCCDs provide equally good results in terms of typical time-series differential photometry (compared with typical CCDs) and that their high speed photometric application is superb. Using PSF shaping techniques, we obtained time series photometric observations with precisions of $\lesssim 660 \mu\text{mag}$ per 180 sec integration. Extending this technique to very bright stars, the potential to reach differential precisions near 10^{-5} per exposure is investigated.

Subject headings: Instrumentation - CCD, Orthogonal transfer CCDs, Photometry

1. Introduction

Charge coupled devices have been in use in astronomy for over 30 years and essentially every observatory in the world offers the observer a selection of CCDs and associated instruments to choose from. Recent advances in CCD technology have mainly been in terms of increased quantum efficiency, radiation hardness, and non-optical applications (see Howell 2000). However, the orthogonal transfer CCD (OTCCD), developed by Tonry et al. (1997, hereafter TBS), offers some interesting new possibilities for photometric observations.

Originally designed for image motion compensation (a “no moving parts” tip/tilt

system), OTCCDs can be used in “OT” mode, shifting charge rapidly (within 100 μ sec) or can be used in normal operation. Due to the complex nature of their gate structure and the fact that during a typical electronic tip/tilt observation, the charge within each pixel may be shifted up to 100 times each second, we were uncertain as to the detailed photometric performance of these arrays. OTCCDs are currently in use in the OPTIC camera (discussed below), a similar single OTCCD clone camera is nearing completion, and OTCCDs will be the type of CCD used in the QUOTA array (8K X 8K) and One Degree Imager (32K X 32K) instruments (see Jacoby et al., 2002) being built for the WIYN telescope on Kitt Peak. The Pan-STARRS¹ survey telescopes will use large OTCCD arrays as well and are expected to be operational near 2006.

The highest precision ground-based photometry to date was obtained using the technique of differential ensemble photometry (see Everett & Howell 2001, hereafter EH) and determining relative brightness measurements for one or more stars within a field of view. EH reached precisions of 2 mmag per few minute integration for point sources using this technique. Similar techniques have been used by a number of groups to obtain high precision light curves of (variable) sources and differential photometry is the preferred method for high precision photometry by which, for example, extra-solar planet transits will be discovered. Here we explore the ability of OTCCDs to provide similar high photometric precisions as those obtained with conventional CCDs and their use as high-speed digital photometers. In addition, using our new technique of point spread function (PSF) shaping, as ultra-high precision photometers.

¹<http://pan-starrs.ifa.hawaii.edu>

2. OTCCDs

OTCCDs are four-phase devices where the fourth phase is not the typical channel stop, but a small implant in each pixel corner allowing the device to perform both horizontal and vertical clocking. Setting the fourth phase low allows the OTCCD to act as a conventional CCD whereby the charge can be clocked down using typical 3 phase techniques. The structure of each pixel is shown in TBS as are the details of the operation and results when used for image compensation. Typical shifts occur at rates of 5-30 Hz and each shift movement is generally a few times 1 pixel. TBS provide a brief discussion of the photometric performance of the OTCCD in terms of charge diffusion and how image improvement increased S/N, but did not explore the ability of an OTCCD to perform time-series or high precision photometric observations. Application of OTCCDs to photometry promises increased precision as charge shifting and shaping increases the electron collection capacity and should average out any efficiency differences and gate structure effects. The ability to produce equal, albeit non-typical, PSFs across the field of view is an additional benefit.

2.1. OPTIC Camera

Our observations were carried out using the Orthogonal Parallel Transfer Imaging Camera (OPTIC - built by one of us [JT] as a prototype OTCCD imager, see Tonry et al., 2002) attached to the University of Hawaii's 2.2-m telescope. OPTIC consists of two 2K by 4K CCID-28 OTCCDs arranged in a single dewar mounted adjacent to each other with a small gap in between the chips (see Figure 1). OPTIC uses standard SDSU-2 electronics build by R. Leach and reads out the CCD via 4 video channels, one located in each corner of the device.

Electrically, each OPTIC OTCCD is divided into two regions (each 2048 by 2048

pixels), and each region is further divided in two; a guide region and a science region. The guide regions sit at the top and bottom of each CCD and are 2048 by 516 pixels each while the science regions are 1536 by 2048 pixels each. The science region occupies the central 3072 X 2048 pixel CCD area. Each CCD is 2048 by 4104 total pixels in size with 15 micron pixels yielding a 9.2 X 9.2 arcmin field of view or 0.135 arcsec/pixel at the University of Hawaii's 2.2-m telescope. OPTIC has a read noise of <4 electrons when read at a normal rate of 160 kpix/sec and a nominal gain of 1.45 e/ADU. Figure 2 shows an image obtained with the OPTIC camera. This image shows the four CCD quadrants and the regions of the OTCCDs which can be used for guiding. One or more guide quadrants can be assigned to guiding using a star suitably positioned within. The used guide quadrants (as the blank region in the lower right) are filled with zeros after readout while non-used quadrants revert to normal science duty.

OPTIC can guide, track and image compensate at rates up to 100 Hz. In tracking/guiding mode, the software reads out a small pixel patch around 1 to 4 guide stars which are located within the guide regions. Centroids are computed for each guide star and a prediction x,y location is generated and used to shift the charge in the science array. See TBS for details as to how the guide stars are used to image compensate through science region charge shifting.

3. Observations and Results

We used OPTIC at the University of Hawaii's 2.2-m telescope located on Mauna Kea during the nights of 2002 December 4-10, 2003 January 21-26, and April 5-9. During the first two runs, tests of OTCCD photometric and astrometric capabilities were undertaken as precursor studies for the Pan-STARRS project. The winter observing conditions were clear but with poor seeing and high winds. The April run was clear with seeing

between 0.6-1.0 arcsec and no wind. April OPTIC observations were roughly split between science observations, mostly of the Virgo cluster of galaxies in which OPTIC was run as a conventional CCD, and photometric tests consisting of conventional time series photometry for comparison purposes, video mode (high speed) photometry, tracking moving objects, and PSF shaping to go after ultra-high precision results. We describe each of our differential photometric tests and their results below.

3.1. Conventional Stare Mode

In order to test the base ability of OTCCDs to obtain time series photometry, we used OPTIC as a conventional 3-phase CCD. One advantage OPTIC has, however, is that the OTCCD's can provide guiding themselves (sending error signals generated from the guide stars to the telescope control software) or can provide fine guiding corrections in addition to conventional telescope guiding, both while performing image compensation. A few fairly crowded star regions were observed through a standard V or R filter and the data were reduced and analyzed as described in EH. A sample result is shown in Figure 3 for R band observations of a random field of view near the star GD66. The results presented in Figure 3 (with precisions of near 1 mmag) as well as the other time series datasets we obtained show that using OPTIC as a conventional CCD provides time series photometric results equally as good or better than those obtained with normal CCDs (see EH).

3.2. Video Mode (High Speed) Photometry

Placing an object of interest in to the guide regions allows one to both guide as well as collect high cadence observations of the source. High speed photometry is now mainly a distant memory in observational astronomy, as it was the realm of photomultiplier

tubes and photo-diodes. CCDs brought two-dimensional photometry to observers, but they generally have too slow a readout to provide sampling at time scales less than 10-30 seconds. The general problems encountered are that either the “user” instrument available at an observatory does not allow for fast readout and/or the read noise is not tolerable (or unknown) for a given camera if one were to read at fast rates. Additionally, high speed image production from typical CCD cameras with software to reduce such unconventional image data is not available.

While the guide regions in the OPTIC camera can be read out at rates of up to 100 Hz, we too must be concerned with very high read noise during such fast imaging as well as the structure of the underlying bias when using such rates. Generally, bias levels in a CCD are flat (that is a given DC offset level) and the “noise” of the bias level is the read noise of the CCD (see Merline & Howell 1995). For the fast readout of the OPTIC OTCCDs, we have determined that the underlying bias structure has a constant exponential form which can be well modeled and removed (if desired).

Using guide boxes of size 32 X 32 or 64 X 64 pixels (although any size is allowed), we performed observational tests of video mode photometry with OPTIC. Placing the source of interest in one of the guide regions, preferably as close to the readout amplifiers as practical, we then chose one or more additional guide stars in the remaining three guide regions. The additional stars are recruited to help correct for transparency variations etc. as in normal differential photometry. The remaining science area of the OPTIC OTCCDs acts as a conventional, albeit OT guided, CCD array.

For our video tests, we choose integration times for the science frame of 3-5 minutes, during which the guide regions were readout at rates of 1-10 Hz (100 to 1000 msec). Our limiting video rate was due to photon starvation, which on the UH 2.2-m telescope, occurred near $V=14$ th for 0.4 sec video exposures. OPTIC software for the guide region video frames

produces FITS images, one frame of which is illustrated in Figure 4. Each video image is collected and placed into a single FITS image as an image section. Using software based on that of EH, we then perform differential photometry on the four video stars for each frame in the time series sequence.

Video mode photometry with OPTIC produces very good results as illustrated by an example shown in Figure 5. The light curve presented is a 1 sec sampled R band data set for the eclipsing cataclysmic variable star U Gem ($R \sim 13.5$). Our OPTIC dataset provided nearly one orbital period (4.2 h) of data and included most of the primary eclipse. Figure 6 shows the detail around the eclipse minimum and the photometric uncertainties (error bars) of 0.01 mag per point can be seen. Similar datasets were obtained for the V=14 variable star Sco X-1 using 400 msec exposures in V yielding uncertainties of 0.1 mag, for the V-14 eclipsing binary V893 Sco (400 msec, 0.1 mag uncertainties) and the V=11 variable T CrB (200 and 400 msec, 0.01 mag uncertainties).

There are some minor issues remaining with this observation mode that we are working to solve. The exact start time and length of the exposure are currently not known to better than ~ 15 msec. This is partly due to the location of each guide star within its guide region (which can take from from 1-10 msec for parallel transfer) and partly due to readout time (2-5 msec) plus varying overhead times in the Linux host computer. We are currently modifying our software to produce consistent timing results accurate to near 5 msec.

The chances of finding three other guide stars (ideally) of similar brightness to the object of interest lying within the three other (small) guide regions are low. Thus, we have provided a routine to allow for different integration times within each guide region. This option uses a base time (the shortest integration time) and the user may pick integer multiples of this base time for each of the other guide regions. We are also going to implement an additional feature which will allow each guide region to be placed almost

at random within each 1/2 of each CCD. This will eliminate any “science” region in that quadrant, but that is of no consequence if one desires video photometry.

3.3. Moving Target Photometry

Classically, observations of moving targets (e.g., asteroids) have been done by one of two methods. Either the observer would track at the sidereal rate with the observation yielding round stars and a trailed target or the observer would set the telescope to track at the known or predicted rate of motion of the target and integrate. This latter method produced a round target and trailed stars providing better signal to noise for the object of interest. Some observers used a middle-of-the-road approach, tracking at a rate about halfway between the two.

The method whereby the telescope tracking rate is changed is cumbersome as each source requires a different rate to be placed into the telescope control software and a number of telescopes do not track well or at all at non-sidereal rates. Using the inverse process of guiding with the guide stars, we merely inject RA and DEC offsets into the OTCCD science array at each (guide) time interval which moves the charge within the array at the tracking rate of the (moving) object of interest. The telescope continues to track (and guide) at the sidereal rate regardless of the rate and direction of the moving target, while the image moves across the CCD at the non-sidereal rate.

A simple command containing the tracking rates in mas/s for both RA and DEC (e.g., drift vector 50.1 -2.6) sets the OPTIC charge tracking mode. Figure 7 shows one section of an OPTIC image of the V=17 asteroid 2003 FC5. The left panel shows a sidereal rate 200 sec exposure in which we see the round stars and the tell-tale 60 pixel long trail of the asteroid. The right hand panel shows our OPTIC image in which the charge was moved

on-chip during the 200 sec integration at the rate of the asteroid. Now we see a nice round asteroid and trailed stars. The peak pixel values in the round asteroid image are three times those in the trail, resulting in a signal-to-noise difference between the two images of approximately a factor of 6 for the same integration time.

3.4. PSF Shaping

High precision photometry is a simple concept in principle. Collect N photons and, for large N , the (1σ) precision (in magnitudes) of a measurement is given by $\frac{1.09}{\sqrt{N}}$ magnitudes (Howell 1993). Reality comes into play when one adds two constraints; high precision over a (short) time interval and an understanding of the uncertainties within the high precisions desired. Both of these additional constraints have been solved (see EH) for uncertainties near 1 mmag and it is now a routine matter to achieve time series CCD photometry from the ground which has such precisions. However, we wished to look into both the ability to improve on this precision for normal time series observations as well as push the precision limit to even higher values. Both cases were attempted and both produced highly successful initial test results.

Theoretically, the perfect PSF is a “top hat” shape. Models such as that presented in Merline and Howell (1995) show that this shape, with steep sides and a flat top, would yield the highest S/N for all imagined shapes, and clearly provide higher precision than a typical, azimuthally symmetric, near Gaussian PSF. However, modeling attempts by one of us (SH) related to “fitting a round peg into a square hole”, revealed that a modified top hat or “mesa” shape would provide a simpler shape to make when imaging onto the square pixel grid of a CCD. To this end, we developed software to move the charge in the OTCCD science array in a square pattern during an integration. We apply to each exposure a sequence of x,y pixel offsets which move the science array charge (and thus all imaged

objects) in a square pattern. The details of our initial PSF shaping test include three user input numbers to the software; the box size in x and y pixels, and the number of times to transverse the entire box during each total science integration. The raster scanning is not a continuous process and too large of a box or too many (or too few) repeats for a given integration time will lead to highly non-uniform, sparsely populated, or locally saturated square star results.

At each video iteration (the video [or guide] rate is set by the user), the charge located in the science array is moved in a raster scan according to the following prescription,

$$\text{Total Path Length} = N_{\text{Repeats}} \times x_{\text{box size}} \times y_{\text{box size}} \quad (1)$$

where a given charge sample at time t corresponds to a location within the specified box determined by

$$\text{Location} = \frac{t}{\text{Science Frame Integration Time}} \times \text{Path Length}. \quad (2)$$

We then convert Eq. 2 back into an x,y position ($\text{Location}/2 = x$, $\text{Location}/2 = y$) and very rapidly shift the charge at each quasi-random location within the $x_{\text{box size}} \times y_{\text{box size}}$ PSF shaped box. A prudent choice of N_{Repeats} (generally a small number) and box size will provide ideal tessellation of the PSF and cover all possible locations, thus uniformly filling the PSF shaped box during each science frame integration time. There can be some interesting looking images produced by the beating of or poorly chosen input parameters, the guide rate, and the science frame integration time, however most are not scientifically useful. We are developing a better charge motion algorithm and a method to estimate ahead of time reasonable choices for N_{Repeats} , $x_{\text{box size}}$, $y_{\text{box size}}$ and the integration time, based on star brightness, plate scale, and telescope aperture.

The PSF in any optical system is a function of location with respect to the optic axis, color, and time. PSF shaping (a form of controlled dithering) reduces the effects just

listed by providing a smoothing function leading to a more uniform PSF. This method has advantages over simply de-focusing. Moderately de-focused images have been tried as a method of obtaining better photometric precision (e.g., see Gilliland et al., 1993) and provide some increases. Slightly de-focused images will be used in the upcoming Kepler Discovery mission as well, as a method of softening the instrumental PSF to avoid saturation. De-focusing spreads light out producing a “doughnut” type PSF which is location dependent and reveals numerous color and optical aberrations in the image. Power for a given object is shifted out of the higher S/N core region into the larger lower S/N wing region. PSF shaping has none of these disadvantages and can provide ultra-high photometric precisions in each single exposure by greatly increasing the number of collected photons (N) without saturation worries. N is approximately equal to the total number of pixels in the PSF shaped box ($x_{box\ size} \times y_{box\ size}$) times $\sim 80\%$ of the pixel full well capacity (assuming one is still in the linear range).

We first tried a simple test of producing square stars by PSF shaping a star field for which we had observations obtained in conventional mode. Figure 8 shows one quadrant of a full image obtained with the OPTIC camera which has been PSF shaped in to 30 X 30 pixel boxes with $N_{repeats}=10$. We used 180 sec integrations (science region), an I band filter, and a guide rate of 50 msec to obtain a PSF shaped time series data set of this field which contains the variable star VV Pup. Figure 9 shows a 3-D plot of one of the PSF shaped stars revealing its mesa appearance.

Using a slightly-modified version of the EH code (to operate on square stars), we performed aperture ensemble differential photometry on our short (2 hour) time series test. In this case, we chose each star ”by eye” to avoid crowding and CCD edge effects and used circular apertures (50 pixels or 6”8 in diameter) to enclose the entire square PSF of each star. The apertures just included the PSF corners which are 42 pixels from the PSF

center. We plot the standard deviation in magnitudes measured for each light curve versus instrumental magnitude in Figure 10. This plot can be compared with that in Figure 3, our time series observed in conventional fashion. By using shaped PSFs, we are able to achieve higher precision photometry in the brightest stars. This is in part due to our ability to collect a larger number of photons without saturating the CCD and the production of better flat fields. Noisy and possibly non-linear pixels (or deferred charge effects) in the wings of normal round PSFs are avoided and help improve the result as well. The brightest stars in this time series were observed with photometric precisions of $400 \mu\text{mag}$ (4×10^{-4}) per 180 second exposure at I using shaped PSFs, while we observed a best photometric precision of 1.5 mmag at R using conventional PSFs. The higher precisions do come at the trade-off of noisier light curves for the fainter stars in the shaped PSF data for which the large apertures caused an increase in the noise contribution from the sky. Very faint or extended sources or those with low surface brightness may be lost completely in this mode.

Figure 11 shows the light curve of one of the bright constant PSF shaped sources in our I band time series. The individual 1σ uncertainties per datum are $400 \mu\text{mag}$ while the standard deviation of the light curve is $660 \mu\text{mag}$. This latter value is what we quote as our precision for the measurement. The modulations observed in the light curve may be real or could be remaining systematic effects we need to understand and have not yet fully compensated for. We see roughly equal amplitude but dissimilar (apparently random) patterns in all the bright ensemble stars used here. At this level of precision, many stars may be variable and we must gain further experience with the instrument and technique before we can decide.

Our main objective in PSF shaping, however, was to explore the possibility of obtaining photometric precisions far better than previous attempts. We realized that in order to do this, we'd need to observe bright stars in order to collect large numbers of photons per

unit time. We attempted to observe the bright star BS 90068, chosen due to its magnitude ($V=7$) and its placement in the sky at the time of our tests. BS 90058 was simply too bright to experiment with on a 2.2-m telescope (saturating even 1 sec exposures) so we concentrated on a nearby bright companion ($3.7'$ to the NW at PA=18 degrees) which was about one magnitude fainter ($V=7.8$). Taking a normal exposure, this star saturated (in its core) the OTCCD in 4 sec. To observe in a conventional way would require 3 sec exposures, a OTCCD readout time of 25 seconds (unbinned) and would result in the collection of $\sim 10^6$ photons per exposure. At best, this type of observation can produce photometric precisions of ~ 0.001 mags per 3 sec integration with a very poor on-source duty cycle.

We invested considerable time attempting a number of observations of this star using our PSF shaping technique. Trying different box sizes and $N_{repeats}$ values, we finally settled on a set which worked well. Using a box size of 200 X 200 pixels (30 arcsec on a side), $N_{repeats}=2$, and a guide rate of 50 ms, we obtained 100 sec exposures of the star without saturation. This immediately increased the duty cycle to 68% while producing a PSF which was mesa shaped. Figure 12 shows one of our PSF shaped images of the bright star near BS 90068. Figure 13 shows a 20 column average horizontal cut through the mesa PSF showing how steep walled it is and the level of flatness achieved for the top while Figure 14 shows a false color image of the PSF shaped profile.

Our PSF shaping tests on BS 90068's neighbor obtained 21 exposures over a 30 minute time span which began with thin clouds and ended with thicker clouds and sunrise. Each sky subtracted 100 second image collected $1.1 - 1.4 \times 10^9$ photons for the star. Using \sqrt{N} statistics each image would provide a photometric uncertainty near 2×10^{-5} . This level of photometric precision, *if we can routinely collect and calibrate it*, is high enough to detect Earth-sized planets transiting G type stars. The level of photon flux recorded should, for a constant star and as a proof of the ability to achieve $\frac{1}{\sqrt{N}}$ precisions, remain constant

within $\pm\sqrt{N}$ for observations with errors dominated by photon statistics. Our time series observations, however, did not have photometric conditions and thus can not yet be certain that we can achieve stable photometric precisions of 10^{-5} about a constant mean. We plan additional tests of this bright star PSF shaping technique.

We have much work to do in understanding the complete details of this type of observation, especially in terms of the development of methods which allow precise calibration of the systematics (i.e., differential techniques) at such extremely small uncertainties. At these ultra-high precision levels, we need to find ways of knowing what is constant and what may be varying. The usual culprits of the atmosphere transparency as well as the telescope are to be expected but an even deeper understanding of the instrument, its calibration, and its electronics are needed in order to achieve precisions at the 10^{-5} level.

For example, the on-chip amplifier is probably not linear at better than the 1% level. If we are working strictly differentially (differencing one star against others to look for say a 0.002 mag dip from a planet transit), we know already that we can correct for any constant effects in the amplifier to first order (see EH and Fig. 10). But what effect will issues such as a lumpy PSF mesa (due to seeing changes during the exposure that will effect the central brightness and the wings of the PSF) or a non-uniform mesa top (say with bumps rising to 50,000 ADU within a sea of 30,000 ADU pixels) have on the results? How will other systematics, such as flat fielding differences between different locations on the OTCCD, bias changes, amplifier heating, gain variations, A/D conversion etc. influence the results? In summary, what quantitative effects will limit the photometric precisions and accuracies we can obtain? Let us examine a few possibilities.

4. Noise Source Summary

4.1. Amplifier Nonlinearity

Figure 13 shows that our shaped PSF is not a flat-topped mesa, but shows a substantial variation because of the discrete number of locations where the natural seeing PSF was placed. In this figure, the mean value is approximately 40,000 ADU, and rms variation is approximately ~ 3000 ADU. We could imagine however, that the natural seeing suddenly got much worse and the mesa became very constant at 40,000 ADU. The question then arises as to how much amplifier non-linearity will cause our signal to vary as a function of how flat-topped our shaped PSF is.

Let us imagine that we have a signal whose mean is 1 and which has a random component r , i.e. the star intensity over the shaped PSF is $x = 1 + r$, where r is a Gaussian random variate with rms σ . We imagine that we have an amplifier response $s(x)$ which is what we actually measure and integrate over the area of the mesa.

Then the mean response we get will be

$$\langle s \rangle = \langle s(1 + r) \rangle = s(1) + \left\langle \frac{ds}{dx} r \right\rangle + \frac{1}{2} \left\langle \frac{d^2s}{dx^2} r^2 \right\rangle \quad (3)$$

to second order. This simply becomes

$$\langle s \rangle = s(1) + \frac{1}{2} \frac{d^2s}{dx^2} \sigma^2. \quad (4)$$

For example, we might imagine that $\sigma = 0.08$ as in Figure 13, and a plausible amplifier response might be $s(x) = x - \alpha x^2$, where $\alpha = 0.01$, i.e. the amplifier is 1% non-linear at the signal of interest. From this we see that the difference between a measured signal when $\sigma = 0$ and $\sigma = 0.08$ is

$$\alpha\sigma^2 = 0.01 \times 0.08^2 = 6 \times 10^{-5}. \quad (5)$$

The amplifier linearity may also be a function of its history, that is what the prior pixel value was. Starting around the 10^{-4} level we will need to measure the amplifier response in more detail in order to avoid a systematic error arising from the details of the shaped PSF, and we believe that we can do a good job of correcting for these effects to the 10^{-5} level.

4.2. Flat Fielding

Flat fielding comes into play in a few different but related ways in an OTCCD PSF shaped image. The usual dome or sky flats provide information about pixel to pixel variations but once one begins to look in detail at a PSF, the relative sensitivities of the (intra-) pixel gate structures may be of concern. For differential referencing, if all stars remain fixed in x,y location, pixel variations are of little importance as they are a systematic source that gets accounted for. However, for observations made on different nights or even for those in which the PSFs move slightly, we need to be concerned about the contributions to the uncertainties that our limited knowledge of each pixel’s QE adds to the final result.

While time series observations obtained over many nights appear not to show offsets which might be caused by flat field uncertainties (EH), we now need to explore this scenario at levels about 100 times more precise. For *well sampled* data, that is, PSFs with a sampling parameter $r = \frac{\text{FWHM}}{\text{pixel size}} > 2.0$, it was shown by Howell et al. (1996) that intra-pixel effects will be averaged out by the seeing disk during an integration. This argument assumes that the the star’s x,y location remains fixed and the seeing does not change radically, especially getting better, during the time series. Differencing any star against an ensemble of others (see EH) averages this effect even further. Large area dithering, as done by the PSF

shaping process, provides even more relief as many gate structures and pixels are averaged over when the PSF is placed at numerous sampling locations. Even the sharp edges of the PSF mesa, have a 6-10 pixel cross section or ~ 1 -2 (normal) FWHM. For all practical x,y locations of a well sampled PSF, this “worst case” can only occur in the low count rate wings. For very large N sources such as that shown in Figure 12, these wing pixels provide only 0.1% of the average flux/per pixel or $\sim 10^{-7}$ of the total collected signal.

EH used 120 flat field exposures of $\sim 40,000$ ADU each to produce a master flat with a fractional uncertainty of 5×10^{-4} (S/N=2000) per pixel. A more usual number of flats obtained (say 10) provides an uncertainty of near 2×10^{-3} (S/N=500) per pixel. What level in the flat field will be required in order to not degrade an observation desiring $\sim 10^{-5}$ precision? The analysis herein needs to proceed on a per pixel basis as that is our smallest unit of digital information we get from the camera.

For the PSF shaped star in Figure 12, we find that the average pixel value within the box is about 45,000 ADU. This count level provides a S/N per pixel of ~ 250 . Using equation (25) in Merline and Howell (1995) (also see Eq. 19 in Newberry 1991), we find that flat fielding will produce a S/N_{out} for each pixel which starts with a S/N_{in} in accord with the relation

$$S/N_{out} = \left[1 + \left(\frac{S/N_{in}}{S/N_{flat}} \right)^2 \right]^{-1/2} \times S/N_{in}. \quad (6)$$

The S/N of the entire measurement will be degraded by the quadrature sum of all the flat field uncertainties for all the pixels within the PSF shaped box. Thus, Eq. (6) tells us that for each pixel, the flat field must have an uncertainty of no worse than about $\sim 10^{-3}$ assuming the flat field uncertainties are both Gaussian and equal for all pixels. This level of uncertainty is easily obtained per pixel using a normal medianed master flat produced from

a collection of 10 or so high S/N flat field frames. We ignore, in this argument, any color differences between the sky and dome flats. While these differences have been explored (see Djorgovski 1984; Tobin, 1993), they have not been examined at the levels needed for our work. In fact, issues related to color differences in the stars themselves are in need of examination as well.

4.3. Atmospheric Scintillation

Atmospheric scintillation (seeing) was discussed in detail years ago in the seminal paper by Young (1974) based on PMT observations and the then current best atmospheric models. Application of this work often uses a simplified version of Young’s scintillation formula to calculate the likely limit as to the best photometric precisions possible for a given telescope aperture and altitude of the observing site. An example of the standard Young formula yields a “scintillation limit” for a few-minute integration with a typical 1-m telescope on Kitt Peak of near 0.0004 mags under the best of conditions. Note, this is the level of precision of our best measurements shown in Fig. 10.

However, recent theoretical work aimed at high precision adaptive optics applications by Heasley et al. (1996) and Ryan and Sandler (1998) concluded that there is no hard fixed limit and it is the conditions of the upper atmosphere that are important for scintillation calculations. These authors, as well as Dravins et al. (1997a; 1997b; 1998) suggest that the best method of measuring, and thus correcting for atmospheric unsteadiness (i.e., the isoplanatic patchiness), is to make use of local reference stars (i.e., a local ensemble). Using this local ensemble, a factor of three reduction in the “Young limit” may be possible. Additionally, scintillation is highly color dependent, $\sigma_S^2 \propto \lambda^{-7/8}$ with $\sigma_S^2(Blue) \sim 2 \times \sigma_S^2(Red)$.

4.4. Other Effects

At the level of discrimination available to the A/D converter (about $2 e^-$ at best these days), the digitization noise can become important when using CCDs with either large values for the gain (G) or when high precision results are required. The contribution to the total noise in a photometric measurement due to the digitization noise is given by (see §2G in Merline & Howell 1995)

$$Noise_{dig} = \sqrt{n_{pix} \times G^2 \times \sigma_f^2} \quad (7)$$

where n_{pix} is the number of pixels used in the star aperture and σ_f is the uncertainty in estimating the true mean of the distribution of the fractional count per pixel, f , within the A/D digitization process. For the OPTIC camera and $n_{pix}=2.1 \times 10^4$ pixels (see Fig. 12), the digitization noise provides only 200 total electrons of uncertainty per integration.

Heating of the A/D due to current flow as readout occurs, can produce small gain or apparent QE changes in the pixels on the CCD. Particularly of concern would be when large count rate transitions occur, such as at the edges of the PSF shaped mesa. We have not yet measured this effect for the OPTIC camera and our PSF shaped stars, but are aware that we may need to as a part of the overall process.

Differential refraction (DR) is another area yet to be fully explored. This comes into play in three ways: If the stars fall on different pixels on different nights, what are the relative color differences in these pixel QE response?; Can the changing temperature of the A/D cause color dependent effective QE changes?; and What about the more normal idea of DR in which stars are imaged through different lines of site (atmosphere and/or clouds) which may have (non-grey) color dependent structure at small levels.

We are just beginning to explore the world of ultra-high precision measurements with OTCCDs and have a number of details to fully understand. However, our photometric tests with the OTCCDs in the OPTIC camera have provided very encouraging initial results. Details and control of the systematics seem to be well in hand and easily controllable at 10^{-3} levels (EH). We have presented strong evidence that precisions near 10^{-4} will now become routine as well using the PSF shaping technique. We need to gather extended data sets in photometric weather to provide certainty of the results presented as well as proof of the ability to collect stable precisions near 10^{-5} . We are also planning observational tests of OTCCDs in the areas of high resolution and high speed spectroscopy.

Development and proficiency in the use of, and software techniques for data reduction and analysis of images from OTCCDs will be needed to allow for efficient and effective use of the new set of large format array imagers being developed. Standard differential photometry techniques took nearly 10 years to become routine at 10^{-3} precisions, hopefully our past experience will allow 10^{-5} precisions to be routinely realized in less time.

The authors wish to thank the members of the Pan-STARRS project who have been very supportive of this work and the University of Hawaii 2.2-m staff and the employees at Hala Pahaku for providing their usual excellent service. We thank George Jacoby for his comments on the manuscript. Partial support of this research has been made possible by NSF grant AST97-96150.

REFERENCES

- Dravins, D., et al., 1997a, PASP, 109, 725.
- Dravins, D., et al., 1997b, PASP, 109, 173.
- Dravins, D., et al., 1998, PASP, 110, 610.
- Djorgovski, S., 1984, in “Proceedings of the Workshop on Improvements to Photometry”, eds. W. Borucki & A. Young, NASA Conf. Pub. 2350
- Heasley, D., et al., 1996, PASP, 108, 385.
- Everett, M. E., & Howell, S. B., 2001, PASP, 113, 1428 (EH)
- Gilliland, R., Brown, T. M., Kjeldsen, H., et al., 1993, AJ, 106, 2441
- Howell, S. B., 1993, in “Stellar Photometry: Current techniques and Future Developments”, Eds. C. J. Butler & I. Elliott, Cambridge University Press, p. 318
- Howell, S. B., Koehn, B., Bowell, E., & Hoffman, M., 1996, AJ, 112, 1302
- Howell, S. B., 2000, “Handbook of CCD Astronomy”, Cambridge University Press
- Jacoby, G., H., Tonry, J. L., Burke, B. E., et al., 2002, SPIE...
- Merline, W., J., & Howell, S. B., 1995, Exp. Ast., 6, 163
- Newberry, M., 1991, PASP, 103, 122
- Ryan, & Sandler, PASP, 1998, 110, 1235.
- Tobin, W., 1993, in “Stellar Photometry: Current techniques and Future Developments”, Eds. C. J. Butler & I. Elliott, Cambridge University Press, p. 304
- Tonry, J. L., Burke, B., E., & Schechter, P. L., 1997, PASP, 109, 1154 (TBS)

Tonry, J. L., Luppino, G., Kaiser, N., Burke, B., & Jacoby, G., 2002, SPIE, ...

Young, A., 1974, ApJ, 189, 587

Fig. 1.— Photograph of the complete OPTIC camera mounted in its (blue) dewar. The two OTCCDs, and the small gap between them, can be seen on the left through the dewar window.

Fig. 2.— This raw OPTIC image shows a 200 s exposure through a V filter of the standard star field near PG0923+129. The OTCCDs are binned 2X2 and one guide region (lower right) was used for guiding during the exposure. On output, the used guide region is filled with zeros. The four science areas (and the three unused guide regions which default to science regions) are easy to identify by their slightly different bias levels. Bad columns are seen in some of the array as well as the gap between the two OTCCDs.

Fig. 3.— Differential time series photometric results for a relatively dense star field observed in 2003 Jan by OPTIC which was used as a conventional CCD. The ordinate represents the 1σ photometric uncertainty in magnitudes for each star’s light curve while the abscissa is the instrumental magnitude which is approximately equal (within 0.5 mag) to real R band magnitudes. Each integration was 300 sec and we obtained 1.5 mmag precisions for the brightest stars and 0.01 mag precision near $R\sim 19$. The solid line is the theoretical expectation, as described in EH, based on the number of photons collected and the instrument and telescope properties. A few variable stars can be identified as they lie well above the theoretical curve.

Fig. 4.— A video mode FITS image as produced by the OPTIC camera software. This single 500 msec V-band image is from a video time-series test on the star V893 Sco, a $V=14$ eclipsing binary. We used 180 sec science frame exposures and observed for over two hours. V893 Sco is the star in the lower left quadrant with the other three being random field stars used to perform differential photometry.

Fig. 5.— A 1 sec sampled, R-band light curve of the $R\sim 15$ eclipsing binary U Gem obtained with OPTIC in video mode. We used a 32 X 32 pixel guide box and extracted the stars

using aperture photometry as described in EH. Each 1 sec exposure produced about 30,000 ADU ($43,500 e^-$) for U Gem.

Fig. 6.— Detailed view of the 1 sec time sampled eclipse of U Gem. The error bars are now apparent (0.01 mag) and a few noisy points can be seen.

Fig. 7.— OTCCD charge tracked image of the $V \sim 17$ asteroid FC5 2003. The left figure shows a normal sidereal rate exposure in which the asteroid is trailed. The right hand figure shows an OPTIC charge tracked image also obtained while the telescope was running at sidereal rate. Both exposures are 200 sec.

Fig. 8.— PSF shaped “square star” OPTIC image of a field near the variable star VV Pup. The PSFs were shaped into boxes of 30 by 30 pixels and $N_{Repeats}=10$. Each exposure was 180 sec in I-band and we used a guide rate of 50 msec. The white squares are charge traps which get shaped as well.

Fig. 9.— A 3-D plot of one of the brighter stars from the previous figure. This image is used to illustrate the mesa shape of the star’s PSF and how well our shaping pattern confines the flux and produces very steep walls.

Fig. 10.— Similar plot to that shown in Fig. 3 but for our time-series using PSF shaped square stars (Fig. 8). This I band sequence used 180 sec exposures and 30 X 30 pixel (4”) boxes to provide precisions as high as $660 \mu\text{mag}$ (6.6×10^{-4}) per 180 sec integration (see text). The instrumental magnitudes are approximately correct and the points near 13.7 and 16.5 are a new and a known variable star (VV Pup) respectively.

Fig. 11.— A light curve of one of the highest precision *constant* stars obtained in the I band PSF shaped time series. The 1σ error bars on each point are $400 \mu\text{mag}$ while the standard deviation of the entire light curve (the value we quote as our delivered precision) is 660

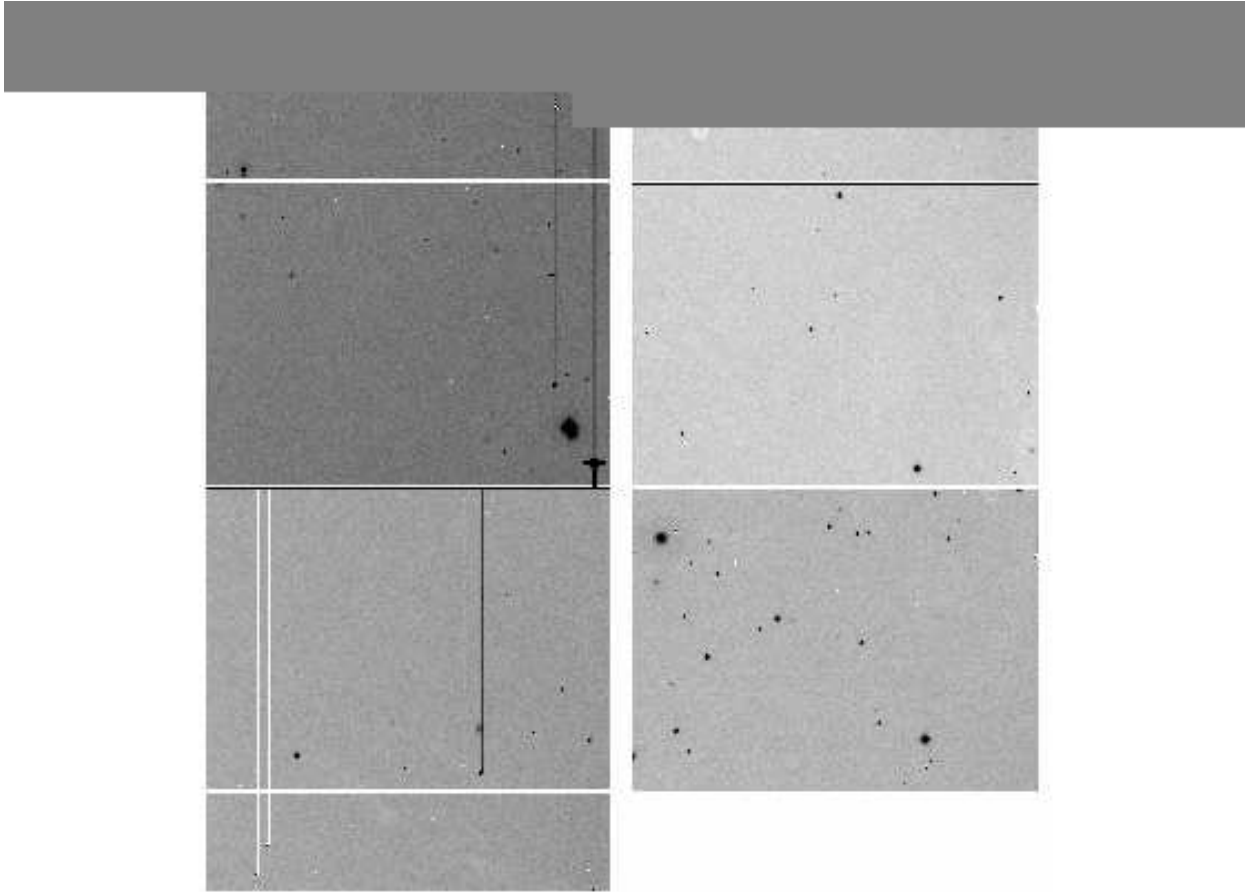
μ mag. The small changes in the light curve *may* be real or they could be uncompensated instrumental effects.

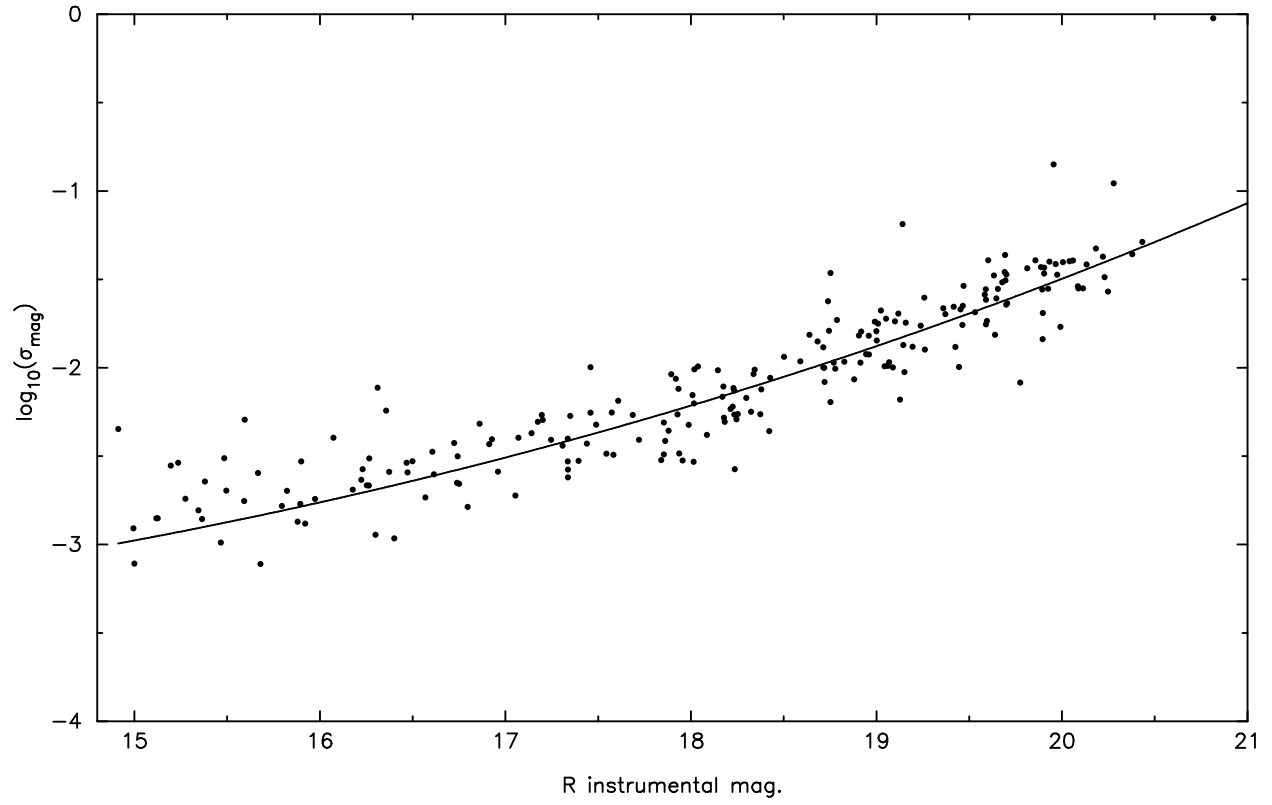
Fig. 12.— PSF shaped bright star in a $N_{Repeats}=2$, 200 by 200 pixel box. This V band image is a $V\sim 8$ star observed for 100 sec with a guide rate of 50 msec and for which we obtained apparent photometric precisions near 10^{-5} per science exposure. The extended halo seen around the square image is the ellipsoid pattern produced by the stellar wings which contain only a small percentage of the total integrated flux.

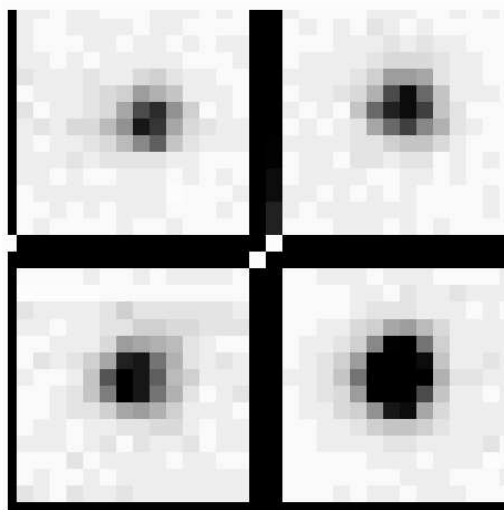
Fig. 13.— A 20 column average cut through the PSF shaped bright star shown in the previous figure. Note the steep sides and fairly flat top of the profile which was obtained during the 100 sec exposure.

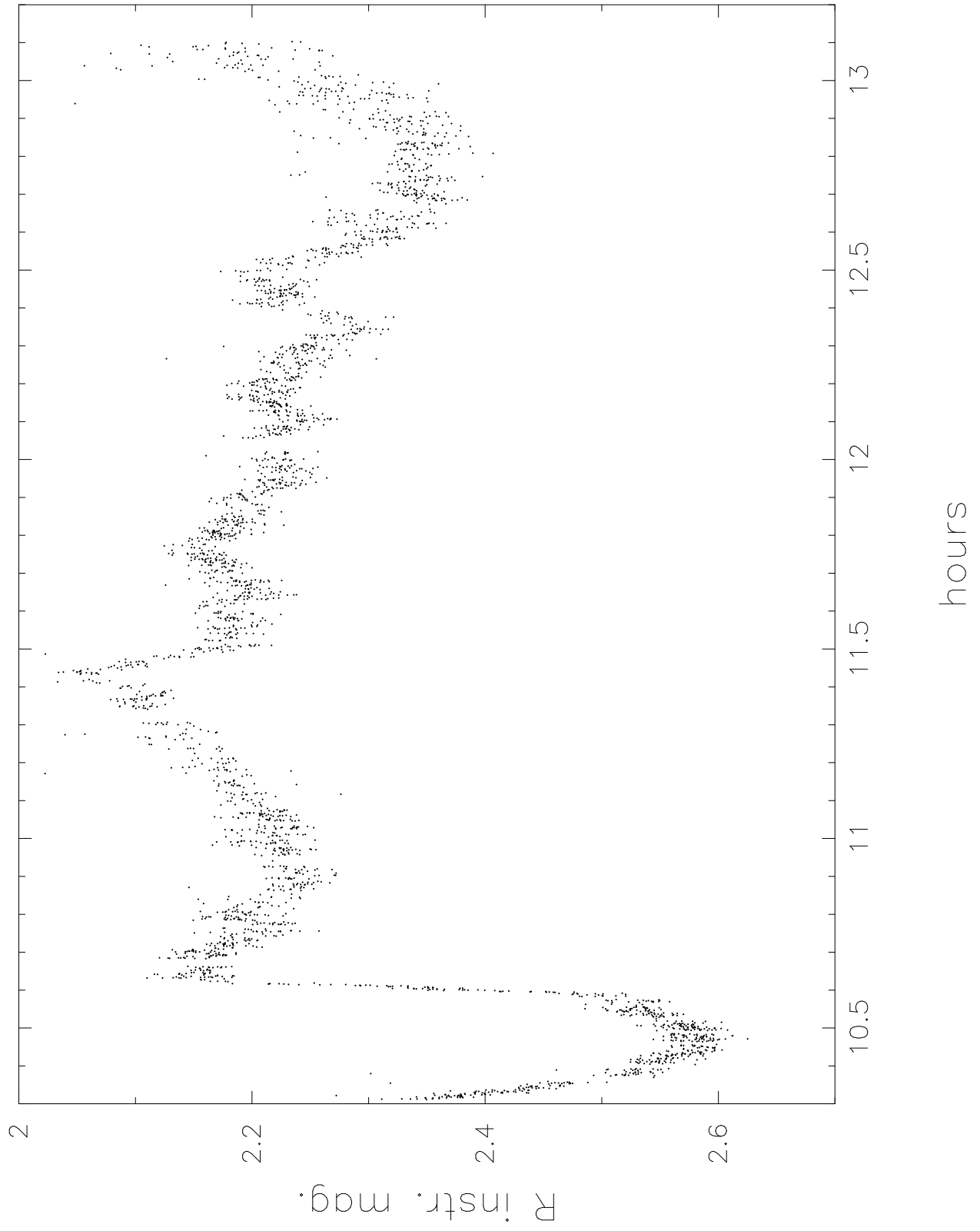
Fig. 14.— A false color image of the mesa profile of the PSF shaped shown in Fig. 12. This image is 290 X 290 pixels in size and the color scale is roughly linear with purple being <650 ADU, blue about 12,000 ADU, green is near $28,000\pm 3000$ ADU and light pink is $>50,000$ ADU.

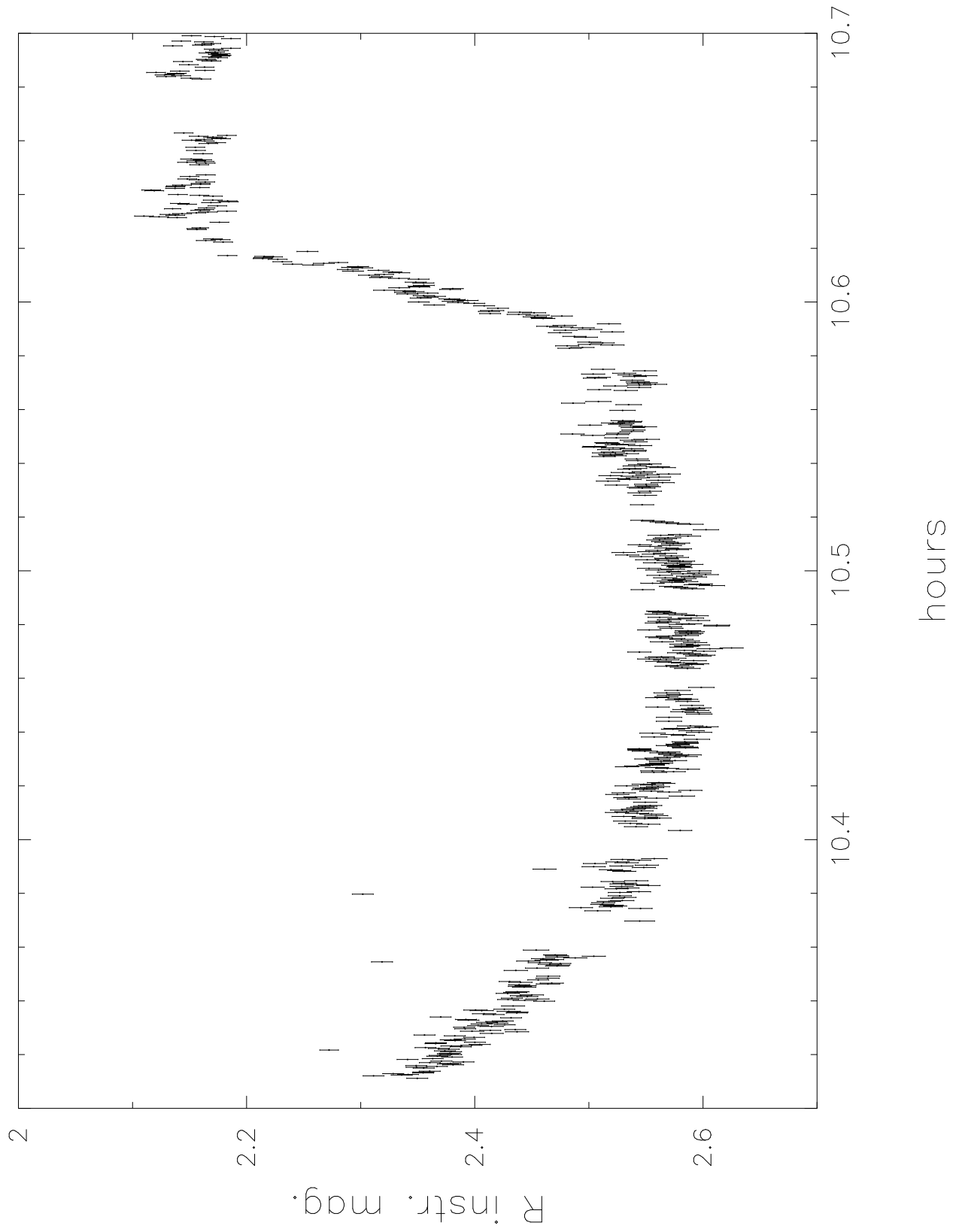


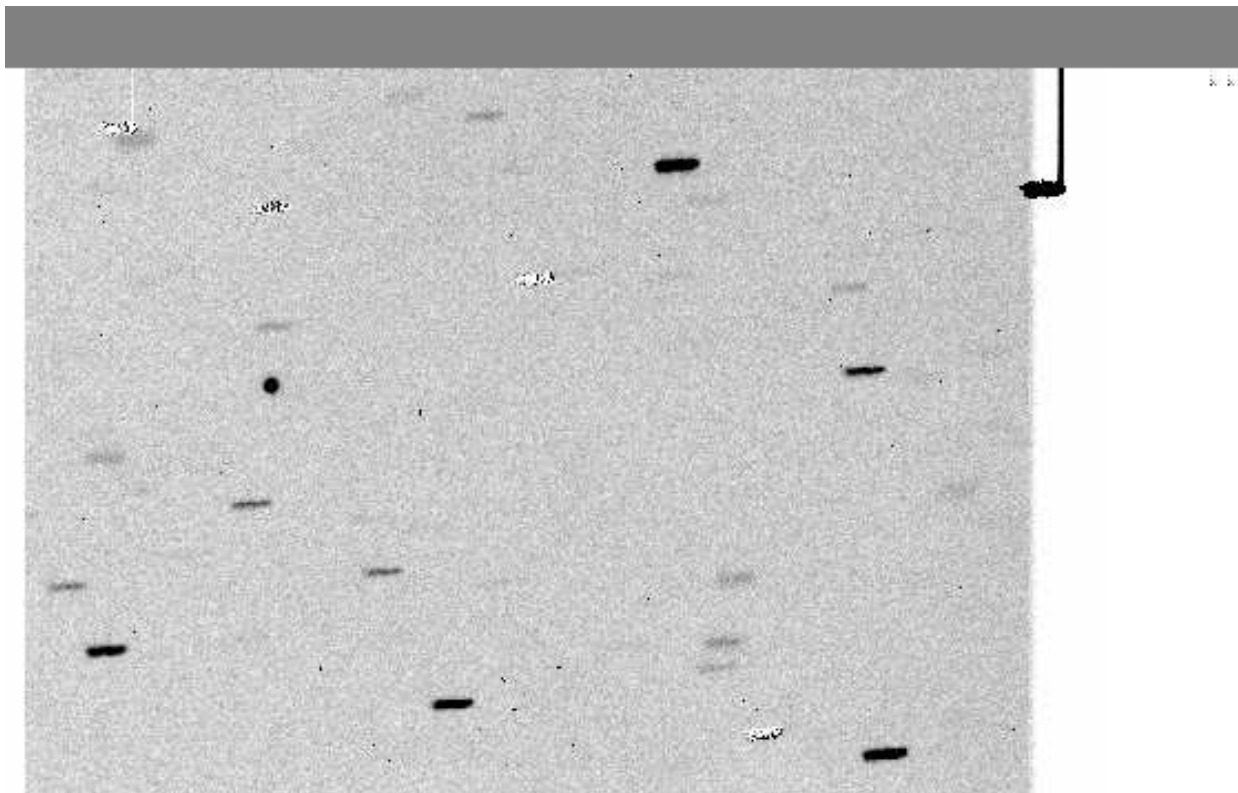


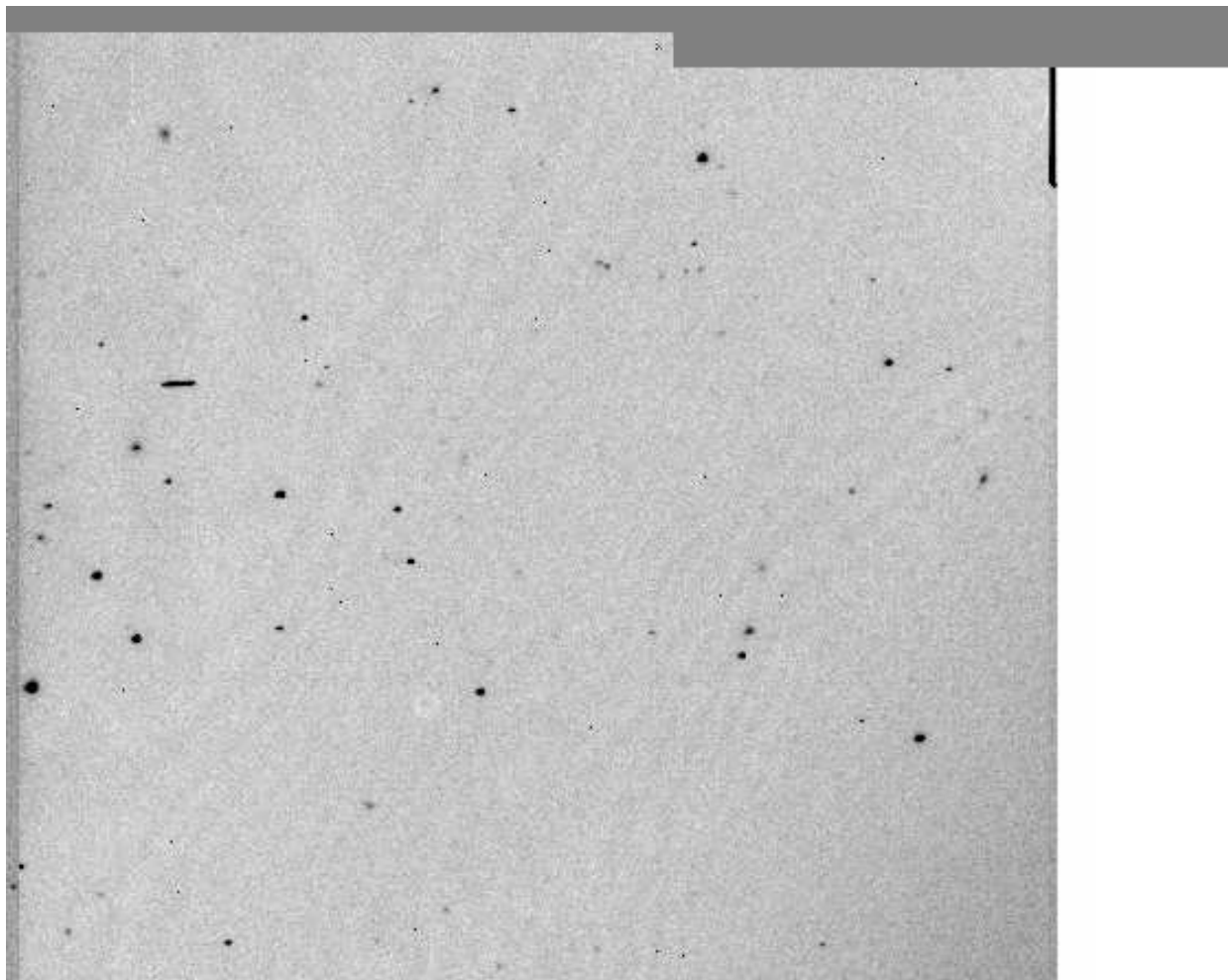


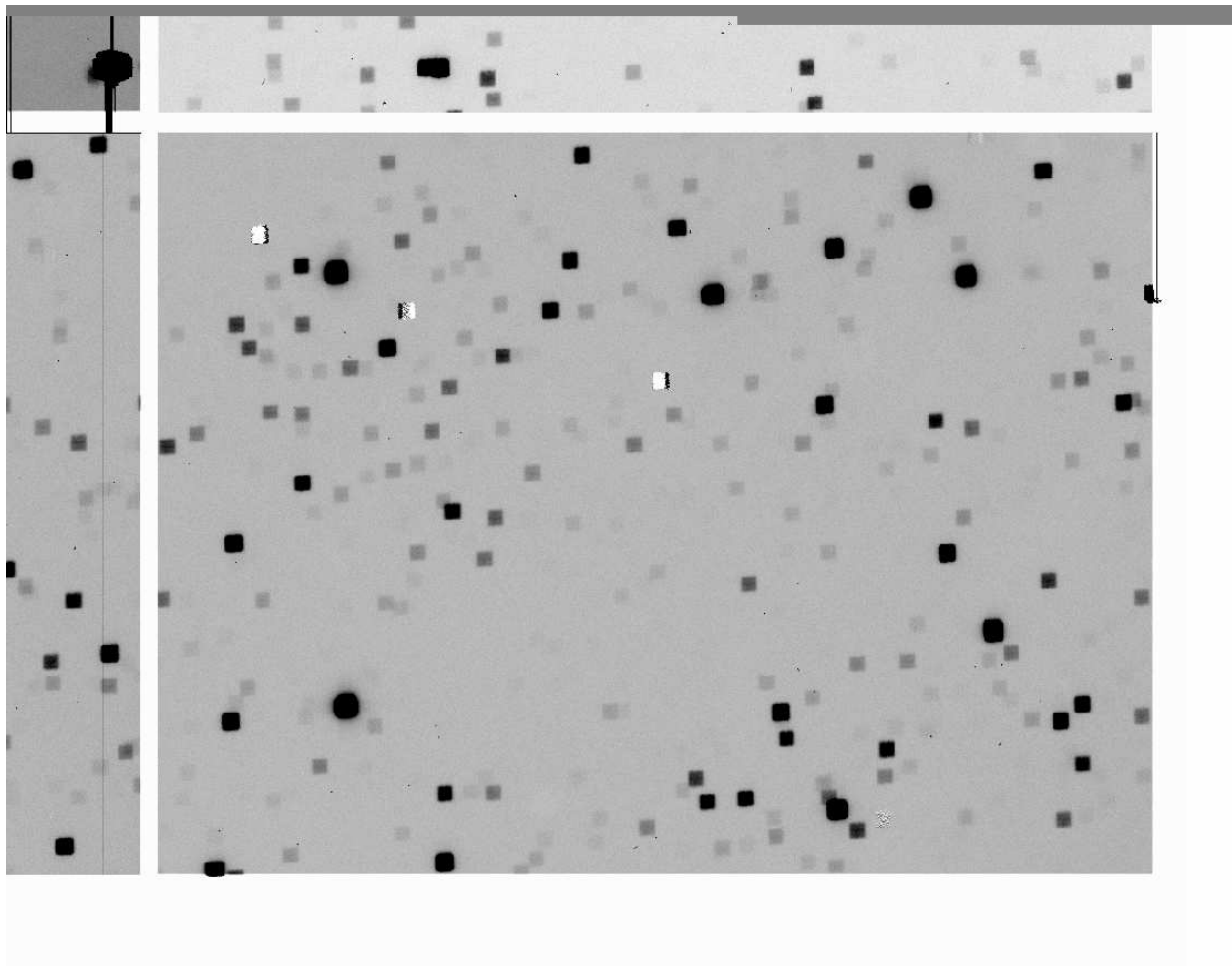












PSF Shaping

